# Multiband Josephson effect in an atomic scale Pb tunnel junction

Maximilian Uhl,[1] Piotr Kot,[1] Robert Drost,[1] Haonan Huang,[1]
Joachim Ankerhold,[2] Juan Carlos Cuevas,[3] and Christian R. Ast[1,*]
[1]*Max-Planck-Institut für Festkörperforschung, Heisenbergstraße 1, 70569 Stuttgart, Germany*
[2]*Institute for Complex Quantum Systems and IQST, Universität Ulm, Albert-Einstein-Allee 11, 89069 Ulm, Germany*
[3]*Departamento de Física Teórica de la Materia Condensada and Condensed Matter Physics Center (IFIMAC), Universidad Autónoma de Madrid, 28049 Madrid, Spain*

(Received 28 May 2024; accepted 23 October 2024; published 3 December 2024)

Multiband superconductivity plays an important role in many emergent novel superconductors and has attracted great interest over the years. Various related experimental aspects have been intensely researched, but a quantitative understanding on the Cooper-pair transport remains still elusive, despite its fundamental and technological importance. We study a Josephson junction with a scanning tunneling microscope (STM), where both tip and sample are Pb, a prototypical type I two-band superconductor. We map the properties of the junction across a wide range of normal state conductances revealing in-gap features originating from multiple Andreev reflections (MARs) and the Josephson effect. We present the theoretical framework to extract the transmission through the transport channels and describe the Cooper-pair tunneling with quantitative precision through two superconducting bands. This paves the way for the understanding of increasingly complicated superconductors.

DOI: 10.1103/PhysRevResearch.6.043233

## I. INTRODUCTION

Josephson junctions form the basis of many emerging quantum technologies. A number of promising implementations of quantum computers, in particular, rely on Josephson junctions for their qubit architectures [1–4]. Applications of the Josephson effect are currently limited to elemental superconductors at sub-Kelvin temperatures [5–7]. Energy efficient and sustainable quantum technologies will require a broader spectrum of available materials with higher critical temperatures.

However, the electronic structure of compounds with higher critical temperatures is often complex. In many cases, more than a single band participates in their superconductivity, which is called multiband superconductivity (MBSC) [8–10]. A thorough understanding of Josephson junctions in MBSC materials is essential to the development of relevant quantum technologies [11–15]. Nevertheless, their complex material nature makes them challenging for fundamental studies.

As an elemental Bardeen-Cooper-Schrieffer (BCS) superconductor with two gaps [16,17], Pb is a rare example and thus an excellent model system to investigate Josephson tunneling in a multiband context. Although the double-gap features in Pb junctions are well documented since the 1960s [18–20], a more detailed understanding on their origin in MBSC was confirmed by means of scanning tunneling microscopy (STM) only rather recently [21,22]. Nevertheless, the interplay between multiband superconductivity and Cooper-pair transport remains elusive.

In this paper, we investigate the Josephson effect in a MBSC environment by studying the tunneling between a Pb tip and Pb(110) surface in an STM. We analyze our experimental data using a quantitative theory, which allows us to disentangle the gap parameters of the single-crystalline sample and the amorphous tip. Combining this with measurements of multiple Andreev reflections (MARs) and including different broadening mechanisms, we extract different transport channels from quasiparticle reference spectra. We use these independently extracted transport channel transmissions to consistently model the Josephson effect, where we reach excellent agreement with quantitative precision with the Josephson measurement. We also assume that the transport channels are in phase.

## II. RESULTS AND DISCUSSION

The tunnel junction consists of a sharp amorphous Pb tip and a Pb(110) surface [Fig. 1(b)]. Pb is a conventional type I BCS superconductor featuring a critical temperature of 7.19 K [23,24], much higher than our experimental temperature of 310 mK [25]. We study the tunneling through such a Pb-Pb junction across a wide range of normal state conductance values by controlling the tip-sample distance [Fig. 1(a)].

At low conductance, the differential conductance ($dI/dV$) spectra reveal the convolution of the tip and sample density of states (DOS) without the effects of higher-order tunneling

*Contact author: c.ast@fkf.mpg.de

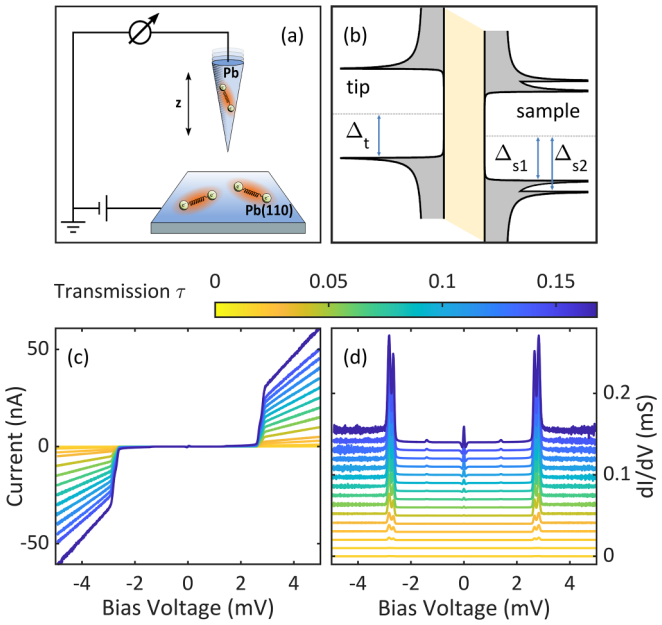


FIG. 1. (a) Schematics of the STM setup with a Pb tip on a Pb(110) surface where the tip-sample distance is varied to change the normal state conductance $G_N$. (b) Density of states as a function of energy in the tip (left) and the sample (right) vertically offset by the bias voltage. (c) Current as a function of bias voltage for different $G_N$ values. (d) Differential conductance $dI/dV$ as a function of bias voltage for different $G_N$ values. The two pairs of large peaks at the gap edge are the coherence peaks showing the two-band nature of Pb. With increasing conductance, the Josephson effect emerges as an increasingly prominent peak at zero bias voltage. The curves are offset vertically by 10 μS for better visibility. The color bar indicates the junction transmission $\tau = G_N/G_0$ for both panels (c) and (d), where $G_0 = 2e^2/h$ is the conductance quantum.

(e.g., Andreev reflections or the Josephson effect) [see Fig. 1(b)]. The measured current and $dI/dV$ spectra are shown as function of bias voltage $V$ in Figs. 1(c) and 1(d) for different normal state conductance values, respectively. Since two bands with different superconducting gap parameters contribute to the superconductivity in Pb, two pairs of peaks at the gap edge are expected in the single-crystalline sample DOS, with gap parameters $\Delta_{s1,2}$. On the other hand, the tip is amorphous [26], so we expect to have only one pair of peaks in the DOS with a gap parameter $\Delta_t$ because of interband scattering, which will be discussed in more detail below. This is evidenced by the observation of only two pairs of coherence peaks in the $dI/dV$ spectra [Fig. 1(d)]. The position and surface dependence of the pairs of peaks has been discussed previously [21].

The quasiparticle current for different values of the junction transmission $\tau = G_N/G_0$, where $G_N$ is the normal state conductance and $G_0 = 2e^2/h$ is the conductance quantum, is plotted in Fig. 1(c). The junction transmission $\tau$ is the sum over the individual transport channel transmissions $\tau_i$, i.e., $\tau = \sum_i \tau_i$. For tunneling between two superconductors at low temperature and low conductance, a current will flow only if the voltage drop between tip and sample exceeds the sum of tip and sample gap parameter [see Fig. 1(c)]. Also, in the $dI/dV$ spectra in Fig. 1(d), a gap around the Fermi level with sharp coherence peaks at $eV = \pm(\Delta_{s1,2} + \Delta_t)$ is observed. At higher conductance values, higher-order tunneling features appear inside the gap. These are MARs, which are the (multiple) reflections of electrons as holes at the superconducting electrodes effectively transferring multiple charges across the junction [27,28]. The lowest-order Andreev reflections give rise to peaks in the $dI/dV$ at $eV = \pm\Delta_t$, $\pm\Delta_{s1}$ and $\pm\Delta_{s2}$. In addition, we observe the Josephson effect, which is the tunneling of Cooper pairs. In the STM, the Josephson effect is strongly influenced by the dynamical Coulomb blockade (DCB) [29–31], which will be described in more detail below. Both processes, Josephson effect and MARs, are clearly visible in gap at high conductance values in Fig. 1(d).

*McMillan model for disordered superconductivity.* Despite Pb being a MBSC material, the amorphous tip results in a single superconducting gap parameter. We can account for this by employing the McMillan framework for MBSC where disorder facilitates coupling and scattering between the bands participating in superconductivity. This leads to a coupling of their gap parameters [32].

In the presence of interband scattering, the gap parameters become interdependent as given by

$$\Delta_i(E) = \Delta_i^0 - \Gamma_{ij}\frac{\Delta_i(E) - \Delta_j(E)}{\sqrt{\Delta_j^2(E) - E^2}}, \tag{1}$$

where $\Delta_i(E)$ is the energy-dependent gap parameter of the $i$th band, $\Delta_i^0$ is the gap parameter of the $i$th band in absence of interband scattering, $\Gamma_{ij}$ is the coupling parameter describing interband scattering, and $E$ is the energy. For bulk crystalline Pb, previous studies have found negligible scattering amplitudes $\Gamma_{ij}$ and thus the spectrum can be approximated by a sum of the two BCS DOSs with two independent unperturbed gap parameters $\Delta_{s1,2} = \Delta_{1,2}^0$ [21].

Amorphous Pb tips show only a single gap because of strong interband scattering as a result of the disordered structure in the tip. This can be nicely explained by the McMillan formalism assuming a strong interband scattering $\Gamma_{ij} \gg \Delta_i^0$. As a result, the coupled equations in Eq. (1) can be solved analytically as shown in Ref. [32], which reduces the two gap parameters to a single effective gap parameter given by

$$\Delta_{\text{eff}} = \frac{\Gamma_{12}\Delta_1^0 + \Gamma_{21}\Delta_2^0}{\Gamma_{12} + \Gamma_{21}}, \tag{2}$$

where $\Gamma_{12,21}$ are hopping parameters between the two bands satisfying $\gamma = \Gamma_{21}/\Gamma_{12} = n_2/n_1$ with $n_{1,2}$ being the normal electronic DOS of bulk Pb near the Fermi level. The DOS is still BCS-like, which means that the order parameter is energy independent and isotropic [cf. Eq. (2)] as opposed to an effectively energy-dependent order parameter as in Eq. (1). From first-principle calculations, we determine that $\gamma = 2.4$ with band 1 accommodating a nearly spherical Fermi surface surrounding the $\Gamma$ point of the Brillouin zone hosting the smaller superconducting gap [16,21]. Consequently,

$$\Delta_t = \frac{\Delta_{s1} + \gamma\Delta_{s2}}{1 + \gamma} \tag{3}$$

with $\Delta_{s1} < \Delta_{s2}$.

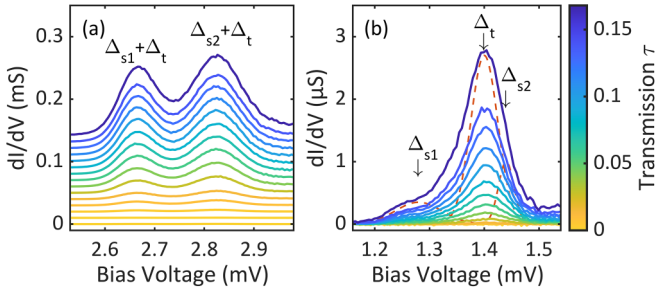


FIG. 2. (a) Zoom in of the double coherence peaks in the differential conductance data of Fig. 1(d) at positive bias voltage for different junction transmissions $\tau$. The graphs are offset vertically with a distance of 10 μS for better visibility. (b) Zoom in of lowest-order Andreev reflection peaks in the differential conductance data of Fig. 1(d) at positive bias voltage $eV = \Delta_{t,s1,s2}$ for different junction transmissions $\tau$ without vertical offset. Because of the close vicinity of the peaks and experimental broadening, the expected peaks merge into one prominent feature with small shoulders on the sides. The red-dashed lines are Gaussians, which act as guide to the eye to illustrate, where the peaks are located. The color bar on the right-hand side shows the junction transmission $\tau$ for both panels.

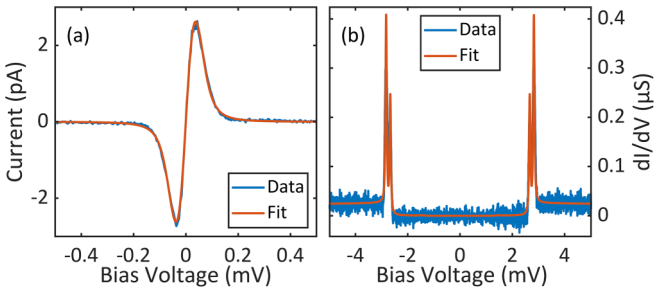


FIG. 3. Low-conductance fits of the Josephson current and the differential conductance spectrum. (a) Fit of the Josephson current by $P(E)$ theory [see Eq. (4)] at a low junction transmission of $\tau = 0.014$ to obtain the parameters of the $P(E)$ function. (b) Quasiparticle fit of the differential conductance spectrum at a very low junction transmission of $\tau = 3 \times 10^{-4}$, where all higher-order tunneling processes are absent.

*Extracting the multiband gap parameters.* The multiband gap parameters $\Delta_{s1,s2,t}$ are essential for the quantitative analysis of MARs and the Josephson effect. Usually, to obtain the gap parameters in tip and sample, the simplest method is to read them directly from the positions of the lowest-order Andreev reflection peaks at $eV = \pm\Delta_{t,s}$ [33]. Here, however, such peaks overlap given the similar values of the three gap parameters $\Delta_{t,s1,s2}$ and the experimental broadening [Fig. 2(b)]. In fact, only one main peak with a small shoulder on its low-voltage side is observed, making it not possible to disentangle all three values precisely just from the Andreev reflection.

Taking into account the coherence peak positions [Fig. 2(a)], we obtain values for $\Delta_{s1,2} + \Delta_t$. Given the theoretical relation in Eq. (3) between $\Delta_t$ and $\Delta_{s1,2}$, we extract the following gap parameters, which are the basis for all further analysis: $\Delta_t = 1.39$ meV, $\Delta_{s1} = 1.28$ meV, $\Delta_{s2} = 1.44$ meV. This result is fully consistent with the lowest-order Andreev reflection peak positions [Fig. 2(b)] corroborating the above theoretical treatment [Eq. (3)].

*Josephson effect at low conductances and the dynamical Coulomb blockade.* Tunnelling through low-capacitance junctions at low temperatures ($T < 1$ K) occurs in the DCB regime, where tunneling is sequential and the superconducting phase is no longer a good quantum number [31]. The interaction of tunneling electrons with the electromagnetic environment becomes important and the Josephson effect is modelled through the $P(E)$ function, which quantifies the energy exchange with the surrounding environment [29,30,33–35]. The $I(V)$ characteristics for the Josephson current in the tunneling limit is given by [31,35]

$$I(V) = \frac{\pi e E_J^2}{\hbar}(P(2eV) - P(-2eV)), \tag{4}$$

where $E_J = \frac{\hbar I_C}{2e}$ is the Josephson energy, $I_C$ is the critical current and the function $P(E)$ describes the probability of the tunneling Cooper pair to exchange a photon of energy $E$ with the environment. The critical current $I_C$ and correspondingly the Josephson energy $E_J$ are given by the Ambegaokar-Baratoff formula, which depends linearly on the normal-state conductance in the low-conductance regime [36]. We model the environmental impedance of the instrument using a phenomenological transmission line model [31]. The parameters in the $P(E)$ function, such as temperature and junction conductance can be obtained through fitting the Josephson current at lowest conductance ($\tau = 0.014$) in the tunneling regime [Fig. 3(a)]. Below, we will extend Eq. (4) to arbitrary conductances, where the $P(E)$ parameters obtained from the fit at lowest conductance will be used as they are assumed to be independent of conductance. In the next step, we disentangle the different transport channels and their respective transmission (i.e., conductance).

*Disentangling the transport channels through MAR fitting.* Quantum transport in the atomic limit proceeds via a small set of conductance channels linking the tip and sample electrodes. The total number of transport channels and their respective transmissions have a profound influence on the junction, especially at high conductance, and must be included in the analysis. Such channel information may be extracted from the subgap structure of MARs as well as the excess current outside of the gap by fitting them to a nonequilibrium Green's function model accounting for MARs as well as multiple transport channels [27,37–41]. Each transport channel couples to a band in the tip and the sample, which leads to four combinations. Because of the different gaps in the sample we have to account for the different DOSs contributing to the different transport channels. In the tip, the DOS is the same in both bands. Treating the transport channels as independent, we model the spectra by two distinctly different signals from the transport channels going to the differently gapped bands, which are superimposed in the measurement. Even though the tip states can be modeled by a single gap, the DOSs are still doubly degenerate owing to the two-gap nature of Pb.

In this analysis, we use the Dynes parameter $\eta$ to account for the effective experimental broadening. To obtain $\eta$, we fit the quasiparticle spectrum at very low conductances where all higher-order processes, including the Josephson effect and

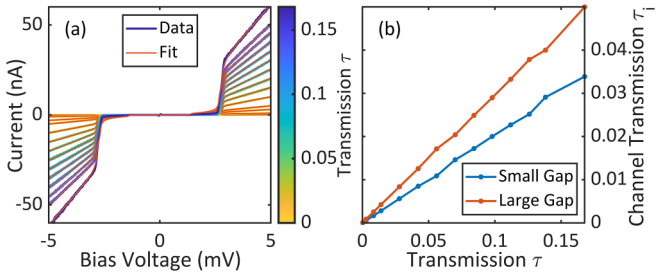


FIG. 4. (a) Multichannel fits of the quasiparticle tunneling current for different junction transmissions $\tau$. The color of each $I(V)$ plot represents their junction transmission $\tau$ as shown in the color bar. The respective multichannel fits are plotted on top in orange. (b) Channel transmissions $\tau_i$ through each of the doubly degenerate channels $\tau_1 = \tau_2$ for the small gap and $\tau_3 = \tau_4$ for the large gap, as a function of the junction transmission $\tau$.

MARs, are absent [Fig. 3(b)]. Here, we assume that $\eta$ for both the tip and sample is the same for simplicity.

Using the parameters obtained from the reference spectra, we perform the transport channel analysis and find the best fits corresponding to a set of two doubly degenerate channels through each of the two bands, resulting in a total of four conduction channels $\tau_1 = \tau_2$ for the small gap and $\tau_3 = \tau_4$ for the large gap. Changing the number of conduction channels leads to dramatically worse results. This result differs from previous measurements [42,43], but we want to point out that the number of transport channels in a tunnel junction can strongly differ depending on the atomic scale properties of the junction. Since these measurements did not mention any multigap superconductivity in Pb, we assume that the measurements were done with polycrystalline Pb in both electrodes. Fits to the data and the corresponding channel transmissions as a function of conductance are shown in Figs. 4(a) and 4(b), respectively. We found that at the moderate junction transmissions presented here, the accuracy of the fit relies more on the excess current outside of the gap than the Andreev reflections inside the gap, which allows us to still obtain reliable results. In addition, the two distinct gaps along with the corresponding coherence peaks allow for a precise determination of the transport channels also at low transparencies.

*Extending the Josephson current model in the DCB regime to arbitrary conductances.* At higher conductances, the Ambegaokar-Baratoff formula and Eq. (4) break down because the current phase relation becomes nonsinusoidal. In addition, the gap parameters in tip and sample are not equal, so that a more generalized approach is needed. To take these aspects into account, the current phase relation for an asymmetric junction at arbitrary transmission for a single channel contact is generally expressed as [40,44]

$$I(\phi) = \frac{8e}{h} t^2 \sin\phi \int_{-\infty}^{\infty} dE \, \mathrm{Im}\left[\frac{f_s f_t}{D(\phi)}\right] n_F(E), \tag{5}$$

where $t$ is the tunnel hopping between sample and tip, $\phi = \phi_s - \phi_t$ is the superconducting phase difference between sample and tip, $f_{s,t}$ are the anomalous Green's functions of the sample and tip, $D(\phi) = \det[1 - t^2 \sigma_3 \hat{g}_t \sigma_3 \hat{g}_s]$, $\sigma_3$ is a Pauli matrix, $\hat{g}_{s,t}$ are the Green's functions of sample and tip in $2 \times 2$ Nambu space, and $n_F(E)$ is the Fermi function. The anomalous Green's function for a BCS superconductor is $f_i(E) = n_i \Delta_i / \sqrt{E^2 - \Delta_i^2}$. The diagonal part of the Green's function is $g_i(E) = n_i E / \sqrt{E^2 - \Delta_i^2}$, so the Green's function becomes $\hat{g}_i = \begin{pmatrix} g_i & f_i e^{i\phi_i} \\ f_i^* e^{-i\phi_i} & g_i \end{pmatrix}$. Note that for a clean BCS-BCS junction, the normal state conductance depends on $t$ through $\tau = G_N/G_0 = \frac{4t^2 n_s n_t}{(1+t^2 n_s n_t)^2}$ where $n_{s,t}$ are the normal state DOS near the Fermi level of the sample and tip [45,46]. Therefore, the current-phase relation is a function of conductance $G_N$. At high conductance, the current phase relation becomes nonlinear in conductance as well as nonsinusoidal, because of the $t$ and $\phi$ dependency of $D(\phi)$ in the denominator. As the tunnel junction of the STM operates in the DCB regime, it is more convenient to express the current-phase relation $I(\phi)$ in terms of charge transfer. Correspondingly, we calculate the Fourier components of the current-phase relation, which is given by

$$I(\phi) = \sum_{m=-\infty}^{+\infty} I_m e^{im\phi}. \tag{6}$$

Using the Fourier components of the current-phase relation, the general $I(V)$ curve for the Josephson current can be written as (see [40])

$$I(V) = 2\pi\hbar \sum_{m=1}^{+\infty} \frac{|I_m|^2}{2me} [P_m(2\,\mathrm{meV}) - P_m(-2\,\mathrm{meV})], \tag{7}$$

where $P_m(2\,\mathrm{meV})$ is the probability for an inelastic process when $m$ Cooper pairs exchanging 2 meV energy with the environment, which is an indicator for multiple Cooper-pair tunneling.

*Multichannel Josephson effect at arbitrary transmission.* Since our transport channel analysis shows the existence of four transport channels, we need to extend Eqs. (6) and (7) to a multichannel situation, where the energy phase relation becomes a sum over different channels [47]

$$I_m = \sum_{c=1}^{n} I_m^{(c)}, \tag{8}$$

in which $c$ denotes the channel number, $n$ is the total number of channels (we assume $n = 4$ here), and $m$ is the number of Cooper pairs being transferred. The Fourier component $I_m^{(c)}$ is then calculated with Eqs. (5) and (6) using the transport channel transmissions from the transport channel analysis performed previously. We note that the transport channel transmissions used in the calculation of the Josephson current are no longer fit parameters, but they are the values from the multichannel fit of the quasiparticle tunneling current in Fig. 4.

In the low-transmission limit, the current-phase relation is sinusoidal and only the $m = 1$ term in Eq. (7) survives. A comparison with Eq. (4) shows that the first-order Fourier component of the energy phase relation satisfies $E_1 = E_J/2$, given the general relation between the $m$th Fourier components of the energy phase relation and the current phase relation $E_m = \frac{\hbar}{2ime} I_m$. Indeed, Fig. 5(a) shows that the Fourier components of the two bands for first order $m = 1$ are close to the respective $E_J/2$ owing to the still comparatively low conductance in the whole measurement range.

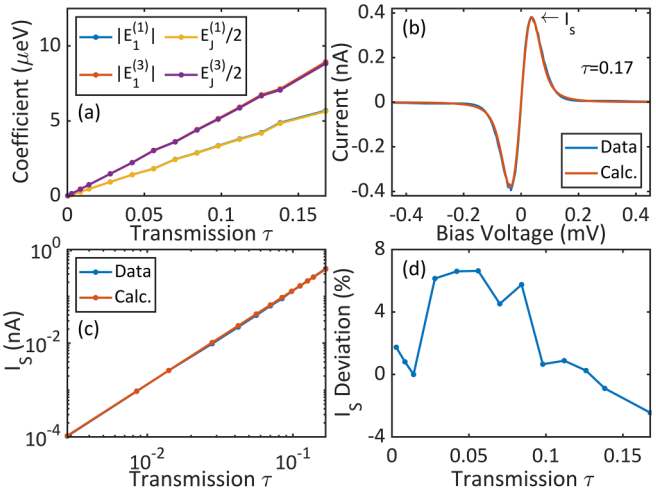


FIG. 5. (a) The first-order Fourier components compared to the Josephson energy $E_J/2$ as a function of junction transmission $\tau$. The blue and the yellow lines as well as the red and the purple lines lie nearly on top of each other. (b) Comparison of the measured Josephson current and the calculation including higher-order Fourier components. The switching current $I_S$ is indicated. (c) The switching current $I_S$ as a function of junction transmission $\tau$ showing good agreement between data and calculation. (d) Relative deviation of the switching current between calculation and measurement, showing only small discrepancies throughout the whole transmission range.

To account for the correction at higher conductances, we use the Fourier components of the current-phase relation up to order $m = 4$ as a function of $G_N$ to directly calculate the full bias voltage-dependent Josephson current [high conductance see Fig. 5(b)]. The calculation agrees with the data well. One important quantity here is the switching current $I_S$, which is the maximum of the bias voltage-dependent Josephson current [see Fig. 5(b)].

We compare $I_S$, which was extracted from the experimental data with the values from the model as a function of normal-state conductance $G_N$, which is shown in Fig. 5(c) To quantify the difference between model and data, we plot the relative deviation in Fig. 5(d). The averaged relative deviation over the whole conductance range is only 2.87 %. This is small considering that the measurement ranges over about two orders of magnitude in $G_N$, which demonstrates the quantitative precision of our analysis of the MBSC Josephson effect.

## III. CONCLUSIONS

In summary, we provide a quantitative understanding of Cooper-pair tunneling processes in a multichannel multiband Josephson junction, which enables the extraction of previously inaccessible microscopic properties of the system. Values that have previously often been combined to single effective values can now be disentangled into their separate contributions. We can distinguish the different gap parameters of the tip and sample bands, and characterize how the supercurrent is distributed over multiple conduction

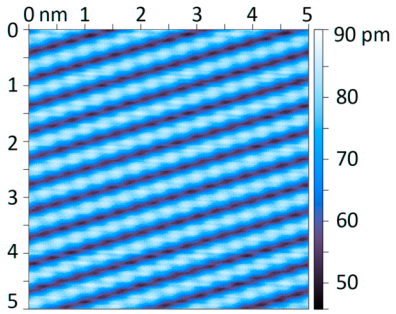


FIG. 6. Topography of the Pb(110) surface. The measured area is representative of the surface and very low in surface defects. The measurements were done on one of the atoms along the lines.

channels through multiple bands. We have reduced the degrees of freedom in the transport channel transmissions by fitting these values from independent quasiparticle current spectra and using them to calculate the Josephson current providing an overall consistent picture.

The agreement between theory and experiment over a wide range of normal state conductance values exhibits a high level of accuracy. The consideration of higher-order $P(E)$ theory, MARs, transport channel analysis, and the above separations of contributions brings the experimental confirmation of the theory to a new level. This improves the understanding of Cooper-pair transport not only through protected quantum states in MBSC [48,49] but also in even more complicated superconductor configurations and their technical applications in the future.

## IV. MATERIALS AND METHODS

*Sample and tip preparation.* The Pb(110) single crystal sample was prepared *in situ* by multiple cycles of alternating between sputtering and annealing. Sputtering was done at an Ar pressure of $5 \times 10^{-6}$ mbar to $6 \times 10^{-6}$ mbar for about one to two hours. Afterwards, for annealing, the sample was preheated in vacuum for about 6 min until it reached a temperature of 250 °C. This temperature was kept for a duration of approximately 30 min. The surface cleanliness was confirmed by measuring a topography as in Fig. 6. The Pb tip was cut from a Pb wire. It was shaped by voltage pulses and dipping the tip into the Pb surface. All measurements were performed in a commercial USM1300 STM system by Unisoku with a base temperature of 310 mK.

*Fit parameters for the P(E) function.* We are using the $P(E)$ function along with a finite transmission line impedance as outlined in Ref. [31]. The junction capacitance is $C_J = 27$ fF, the principal resonance frequency is $\hbar\omega_0 = 54.3$ μeV, the effective damping parameter is $\alpha = 0.4$, the dc resistance is $R_{dc} = 84.6\,\Omega$, and the temperature is $T = 310$ K. In addition, we included a broadening caused by the lock-in amplifier with an amplitude of 10 μeV as well as a general Gaussian voltage broadening with a full width at half maximum of 65.7 μeV.

*Band structure calculations.* We calculate the band structure of Pb by performing *ab initio* density functional theory

(DFT) as implemented in the Quantum ESPRESSO code [50,51], where a plane-wave basis set is used to expand the wave function. Pseudopotentials and the corresponding suggested cutoff energy from Standard solid-state pseudopotentials (SSSP) library are used [52,53]. We use the exchange correlation functional with the generalized gradient approximation (GGA) [54] in the PBE form [55]. The Pb bulk is modeled using a face-centered cubic (fcc) unit cell with periodic boundary condition, where the lattice constant has been fully relaxed until the difference in total energy between consecutive steps is below $10^{-8}$ Rydberg together with an electronic convergence threshold of $10^{-10}$ Rydberg. For self-consistent calculation a $k$ mesh of $[12 \times 12 \times 12]$ is used.

## ACKNOWLEDGMENTS

We gratefully acknowledge stimulating discussions with Alfredo Levy Yeyati, Ciprian Padurariu, and Björn Kubala. This work was funded in part by the ERC Consolidator Grant AbsoluteSpin (Grant No. 681164) and by the Center for Integrated Quantum Science and Technology (IQ$^{ST}$). J.C.C. acknowledges funding from the Spanish Ministry of Science and Innovation (Grant No. PID2020-114880GB-I00).

[1] Y. Makhlin, G. Schön, and A. Shnirman, Quantum-state engineering with Josephson-junction devices, Rev. Mod. Phys. **73**, 357 (2001).

[2] A. Blais, R.-S. Huang, A. Wallraff, S. M. Girvin, and R. J. Schoelkopf, Cavity quantum electrodynamics for superconducting electrical circuits: An architecture for quantum computation, Phys. Rev. A **69**, 062320 (2004).

[3] J. Clarke and F. K. Wilhelm, Superconducting quantum bits, Nature (London) **453**, 1031 (2008).

[4] M. H. Devoret and R. J. Schoelkopf, Superconducting circuits for quantum information: An outlook, Science **339**, 1169 (2013).

[5] J. J. Burnett, A. Bengtsson, M. Scigliuzzo, D. Niepce, M. Kudra, P. Delsing, and J. Bylander, Decoherence benchmarking of superconducting qubits, npj Quantum Inf. **5**, 54 (2019).

[6] G. Andersson, B. Suri, L. Guo, T. Aref, and P. Delsing, Non-exponential decay of a giant artificial atom, Nat. Phys. **15**, 1123 (2019).

[7] N. P. de Leon, K. M. Itoh, D. Kim, K. K. Mehta, T. E. Northup, H. Paik, B. Palmer, N. Samarth, S. Sangtawesin, and D. W. Steuerman, Materials challenges and opportunities for quantum computing hardware, Science **372**, eabb2823 (2021).

[8] A. Bianconi, Multiband superconductivity in high $T_C$ cuprates and diborides, J. Phys. Chem. Solids **67**, 567 (2006).

[9] V. Cvetkovic and Z. Tesanovic, Multiband magnetism and superconductivity in Fe-based compounds, Europhys. Lett. **85**, 37002 (2009).

[10] D. A. Zocco, K. Grube, F. Eilers, T. Wolf, and H. v. Löhneysen, Pauli-limited multiband superconductivity in $KFe_2$ $As_2$, Phys. Rev. Lett. **111**, 057007 (2013).

[11] S.-Z. Lin, Josephson effect between a two-band superconductor with $s++$ or $s\pm$ pairing symmetry and a conventional $s$-wave superconductor, Phys. Rev. B **86**, 014510 (2012).

[12] Y. Yerin and A. N. Omelyanchouk, Proximity and Josephson effects in microstructures based on multiband superconductors (Review Article), Low Temp. Phys. **43**, 1013 (2017).

[13] A. Sasaki, S. Ikegaya, T. Habe, A. A. Golubov, and Y. Asano, Josephson effect in two-band superconductors, Phys. Rev. B **101**, 184501 (2020).

[14] A. Brinkman, A. A. Golubov, H. Rogalla, O. V. Dolgov, J. Kortus, Y. Kong, O. Jepsen, and O. K. Andersen, Multiband model for tunneling in $MgB_2$ junctions, Phys. Rev. B **65**, 180517 (2002).

[15] T. K. Ng and N. Nagaosa, Broken time-reversal symmetry in Josephson junction involving two-band superconductors, Europhy. Lett. **87**, 17003 (2009).

[16] A. Floris, A. Sanna, S. Massidda, and E. K. U. Gross, Two-band superconductivity in Pb from *ab initio* calculations, Phys. Rev. B **75**, 054508 (2007).

[17] H. Suhl, B. T. Matthias, and L. R. Walker, Bardeen-Cooper-Schrieffer theory of superconductivity in the case of overlapping bands, Phys. Rev. Lett. **3**, 552 (1959).

[18] P. Townsend and J. Sutton, Investigation by electron tunneling of the superconducting energy gaps in Nb, Ta, Sn, and Pb, Phys. Rev. **128**, 591 (1962).

[19] G. I. Rochlin, Determination of the anisotropy of the energy gap in superconducting Pb by superconductive tunneling, Phys. Rev. **153**, 513 (1967).

[20] B. L. Blackford and R. H. March, Tunneling investigation of energy-gap anisotropy in superconducting bulk Pb, Phys. Rev. **186**, 397 (1969).

[21] M. Ruby, B. W. Heinrich, J. I. Pascual, and K. J. Franke, Experimental demonstration of a two-band superconducting state for lead using scanning tunneling spectroscopy, Phys. Rev. Lett. **114**, 157001 (2015).

[22] M. T. Randeria, B. E. Feldman, I. K. Drozdov, and A. Yazdani, Scanning Josephson spectroscopy on the atomic scale, Phys. Rev. B **93**, 161115 (2016).

[23] J. Eisenstein, Superconducting elements, Rev. Mod. Phys. **26**, 277 (1954).

[24] B. T. Matthias, T. H. Geballe, and V. B. Compton, Superconductivity, Rev. Mod. Phys. **35**, 1 (1963).

[25] R. Drost, M. Uhl, P. Kot, J. Siebrecht, A. Schmid, J. Merkt, S. Wünsch, M. Siegel, O. Kieler, R. Kleiner *et al.*, Combining electron spin resonance spectroscopy with scanning tunneling microscopy at high magnetic fields, Rev. Sci. Instrum. **93**, 043705 (2022).

[26] P. W. Anderson, Theory of dirty superconductors, J. Phys. Chem. Solids **11**, 26 (1959).

[27] J. C. Cuevas and W. Belzig, Full counting statistics of multiple Andreev reflections, Phys. Rev. Lett. **91**, 187001 (2003).

[28] G. Johansson, P. Samuelsson, and Å. Ingerman, Full counting statistics of multiple Andreev reflection, Phys. Rev. Lett. **91**, 187002 (2003).

[29] M. H. Devoret, D. Esteve, H. Grabert, G.-L. Ingold, H. Pothier, and C. Urbina, Effect of the electromagnetic environment on

the Coulomb blockade in ultrasmall tunnel junctions, Phys. Rev. Lett. **64**, 1824 (1990).

[30] D. Averin, Y. V. Nazarov, and A. Odintsov, Incoherent tunneling of the Cooper pairs and magnetic flux quanta in ultrasmall Josephson junctions, Phys. B: Condens. Matter **165-166**, 945 (1990).

[31] C. R. Ast, B. Jäck, J. Senkpiel, M. Eltschka, M. Etzkorn, J. Ankerhold, and K. Kern, Sensing the quantum limit in scanning tunnelling spectroscopy, Nat. Commun. **7**, 13009 (2016).

[32] W. L. McMillan, Tunneling model of the superconducting proximity effect, Phys. Rev. **175**, 537 (1968).

[33] H. Huang, Tunneling processes through magnetic impurities on superconducting surfaces: Yu-Shiba-Rusinov states and the Josephson effect, Ph.D. thesis, EPFL, Lausanne, 2021.

[34] G.-L. Ingold and Y. V. Nazarov, Charge tunneling rates in ultrasmall junctions, in *Single Charge Tunneling: Coulomb Blockade Phenomena in Nanostructures*, edited by H. Grabert and M. H. Devoret (Springer, New York, 1992), pp. 21–107.

[35] G.-L. Ingold, H. Grabert, and U. Eberhardt, Cooper-pair current through ultrasmall Josephson junctions, Phys. Rev. B **50**, 395 (1994).

[36] V. Ambegaokar and A. Baratoff, Tunneling between superconductors, Phys. Rev. Lett. **10**, 486 (1963).

[37] J. C. Cuevas, A. Martín-Rodero, and A. Levy Yeyati, Hamiltonian approach to the transport properties of superconducting quantum point contacts, Phys. Rev. B **54**, 7366 (1996).

[38] E. Scheer, P. Joyez, D. Esteve, C. Urbina, and M. H. Devoret, Conduction channel transmissions of atomic-size aluminum contacts, Phys. Rev. Lett. **78**, 3535 (1997).

[39] J. C. Cuevas and W. Belzig, DC transport in superconducting point contacts: A full-counting-statistics view, Phys. Rev. B **70**, 214512 (2004).

[40] J. Senkpiel, S. Dambach, M. Etzkorn, R. Drost, C. Padurariu, B. Kubala, W. Belzig, A. L. Yeyati, J. C. Cuevas, J. Ankerhold *et al.*, Single channel Josephson effect in a high transmission atomic contact, Commun. Phys. **3**, 131 (2020).

[41] J. Senkpiel, R. Drost, J. C. Klöckner, M. Etzkorn, J. Ankerhold, J. C. Cuevas, F. Pauly, K. Kern, and C. R. Ast, Extracting transport channel transmissions in scanning tunneling microscopy using superconducting excess current, Phys. Rev. B **105**, 165401 (2022).

[42] E. Scheer, N. Agraït, J. C. Cuevas, A. L. Yeyati, B. Ludoph, A. Martín-Rodero, G. R. Bollinger, J. M. van Ruitenbeek, and C. Urbina, The signature of chemical valence in the electrical conduction through a single-atom contact, Nature (London) **394**, 154 (1998).

[43] J. C. Cuevas, A. Levy Yeyati, A. Martín-Rodero, G. Rubio Bollinger, C. Untiedt, and N. Agraït, Evolution of conducting channels in metallic atomic contacts under elastic deformation, Phys. Rev. Lett. **81**, 2990 (1998).

[44] A. Martín-Rodero, F. J. García-Vidal, and A. Levy Yeyati, Microscopic theory of Josephson mesoscopic constrictions, Phys. Rev. Lett. **72**, 554 (1994).

[45] J. C. Cuevas and E. Scheer, *Molecular Electronics: An Introduction to Theory and Experiment* (World Scientific, Singapore, 2010).

[46] H. Huang, R. Drost, J. Senkpiel, C. Padurariu, B. Kubala, A. L. Yeyati, J. C. Cuevas, J. Ankerhold, K. Kern, and C. R. Ast, Quantum phase transitions and the role of impurity-substrate hybridization in Yu-Shiba-Rusinov states, Commun. Phys. **3**, 199 (2020).

[47] S. Karan, H. Huang, C. Padurariu, B. Kubala, A. Theiler, A. M. Black-Schaffer, G. Morrás, A. L. Yeyati, J. C. Cuevas, J. Ankerhold *et al.*, Superconducting quantum interference at the atomic scale, Nat. Phys. **18**, 893 (2022).

[48] H. Huang, J. Senkpiel, C. Padurariu, R. Drost, A. Villas, R. L. Klees, A. L. Yeyati, J. C. Cuevas, B. Kubala, J. Ankerhold *et al.*, Spin-dependent tunneling between individual superconducting bound states, Phys. Rev. Res. **3**, L032008 (2021).

[49] H. Huang, S. Karan, C. Padurariu, B. Kubala, J. C. Cuevas, J. Ankerhold, K. Kern, and C. R. Ast, Universal scaling of tunable Yu-Shiba-Rusinov states across the quantum phase transition, Commun. Phys. **6**, 214 (2023).

[50] P. Giannozzi, S. Baroni, N. Bonini, M. Calandra, R. Car, C. Cavazzoni, D. Ceresoli, G. L. Chiarotti, M. Cococcioni, I. Dabo *et al.*, QUANTUM ESPRESSO: A modular and open-source software project for quantum simulations of materials, J. Phys.: Condens. Matter **21**, 395502 (2009).

[51] P. Giannozzi, O. Andreussi, T. Brumme, O. Bunau, M. B. Nardelli, M. Calandra, R. Car, C. Cavazzoni, D. Ceresoli, M. Cococcioni *et al.*, Advanced capabilities for materials modelling with QUANTUM ESPRESSO, J. Phys.: Condens. Matter **29**, 465901 (2017).

[52] G. Prandini, A. Marrazzo, I. E. Castelli, N. Mounet, and N. Marzari, Precision and efficiency in solid-state pseudopotential calculations, npj Comput. Mater. **4**, 72 (2018).

[53] K. Lejaeghere, G. Bihlmayer, T. Björkman, P. Blaha, S. Blügel, V. Blum, D. Caliste, I. E. Castelli, S. J. Clark, A. Dal Corso *et al.*, Reproducibility in density functional theory calculations of solids, Science **351**, aad3000 (2016).

[54] J. P. Perdew, J. A. Chevary, S. H. Vosko, K. A. Jackson, M. R. Pederson, D. J. Singh, and C. Fiolhais, Atoms, molecules, solids, and surfaces: Applications of the generalized gradient approximation for exchange and correlation, Phys. Rev. B **46**, 6671 (1992).

[55] J. P. Perdew, K. Burke, and M. Ernzerhof, Generalized gradient approximation made simple, Phys. Rev. Lett. **77**, 3865 (1996).